NASA TECHNICAL NOTE

NASA TN D-4666

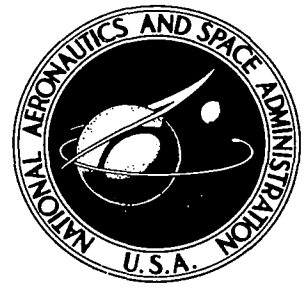

NASA TN D-4666

LUMINOUS EFFICIENCIES OF THREE NICKEL ARTIFICIAL METEORS BETWEEN 9.8 AND 11.4 KILOMETERS PER SECOND

by T. Dale Bess

Langley Research Center
Langley Station, Hampton, Va.

NATIONAL AERONAUTICS AND SPACE ADMINISTRATION • WASHINGTON, D. C. • AUGUST 1968

LUMINOUS EFFICIENCIES OF THREE NICKEL ARTIFICIAL METEORS BETWEEN 9.8 AND 11.4 KILOMETERS PER SECOND

By T. Dale Bess

Langley Research Center
Langley Station, Hampton, Va.

NATIONAL AERONAUTICS AND SPACE ADMINISTRATION

For sale by the Clearinghouse for Federal Scientific and Technical Information
Springfield, Virginia 22151 – CFSTI price $3.00

LUMINOUS EFFICIENCIES OF THREE NICKEL ARTIFICIAL METEORS BETWEEN 9.8 AND 11.4 KILOMETERS PER SECOND

By T. Dale Bess
Langley Research Center

SUMMARY

Results of the experimental measurements of luminous intensity and corresponding luminous efficiency parameters of three nickel artificial meteors are presented. These results are compared with experimental values of iron luminous efficiencies over the same velocity range. All data were reduced from photographs taken with ground-based meteor cameras located at three camera sites operated by NASA Langley Research Center. All flights were from Wallops Island, Virginia, and Nike-Cajun rocket vehicles were used to reenter the artificial meteoroids.

Light curves on blue-sensitive film were obtained for all three nickel meteors, whereas the light curve on panchromatic film was obtained only for the fastest meteor. Data from the third experiment indicated that the radiation for this nickel meteor was strongest in the ultraviolet region of the spectrum; the measured blue-light intensity was about twice that of the panchromatic intensity. The experiments showed that the luminous efficiencies of nickel and iron are about the same at velocities around 11 and 12 kilometers per second; however, for lower velocities the luminous efficiency of nickel is as much as a factor of 10 less than the corresponding iron efficiencies.

INTRODUCTION

One of the parameters associated with the entry of natural meteors into the earth's atmosphere is the luminous efficiency, defined as the fraction of the meteoroid's kinetic energy that is converted to radiation in the region of sensitivity of the detector, at any instant. The luminous efficiency is not easy to evaluate because all the dependent variables are not directly observable. Luminous power radiated by the meteor and velocity of the meteor are observable; however, the kinetic energy of natural meteors is unknown because the mass cannot be determined. Furthermore, the luminous efficiency is expected to be a function of the meteoroid material and density which is also unknown for natural meteors. Therefore, luminous efficiency has not been well determined for natural meteors, and best estimates of this parameter have varied by two orders of magnitude from 2×10^{-2} to 2×10^{-4}. (See ref. 1.)

One of the objectives of the Meteor Simulation Project at the Langley Research Center is to determine the luminous efficiency at the lower meteor velocities. An effective simulation of natural meteor entry into the earth's atmosphere is obtained by using a rocket vehicle system to reenter artificial meteoroids of known mass, density, shape, and material. Ground-based cameras, similar to those used in natural meteor patrols, are used to photograph the artificial meteors. The materials used in the meteor simulation program to date have been iron and nickel, since these two elements are two of the major constituents of asteroidal meteors.

The purpose of this report is to give a brief description of three experiments which utilized a Nike-Cajun vehicle to reenter nickel artificial meteoroids at different velocities, to document the light curves that were obtained from the photographic records, to present the luminous efficiency parameters for the three nickel meteors, and to compare these experimental results with the experimentally determined luminous efficiency of iron meteors.

SYMBOLS

a,b,c,k	constants used in least-squares solution of distance equation
d	distance along reentry trail, kilometers
f	focal length, millimeters
I	radiant power of point on meteor trail, ergs/second (joules/second)
$I_{o,s}$	radiant power of zero magnitude meteor for detectors where s denotes either detector b or p, ergs/second (joules/second)
M	absolute magnitude of meteor
m	mass, grams
t	time, seconds
V	velocity, centimeters/second
τ	dimensionless luminous efficiency
τ_o	luminosity coefficient, seconds/centimeter

τ'_0 luminosity coefficient, second^4/gram-centimeter^3

Subscripts:

b blue-sensitive detector

p panchromatic detector

s refers to type of detector used

v visual detector

DESCRIPTION OF EXPERIMENT

The rocket vehicle system used in the three experiments was an unguided, spin-stabilized, solid-propellant system which utilized a Nike-Cajun booster system to place a velocity package containing two reentry units to an altitude of approximately 110 to 120 kilometers. Each reentry unit was pointed in a rearward direction and was capable of reentering an artificial meteoroid into the earth's atmosphere at a velocity in excess of 9 km/sec. Figures 1 and 2 are sketches of the assembled vehicle and velocity package.

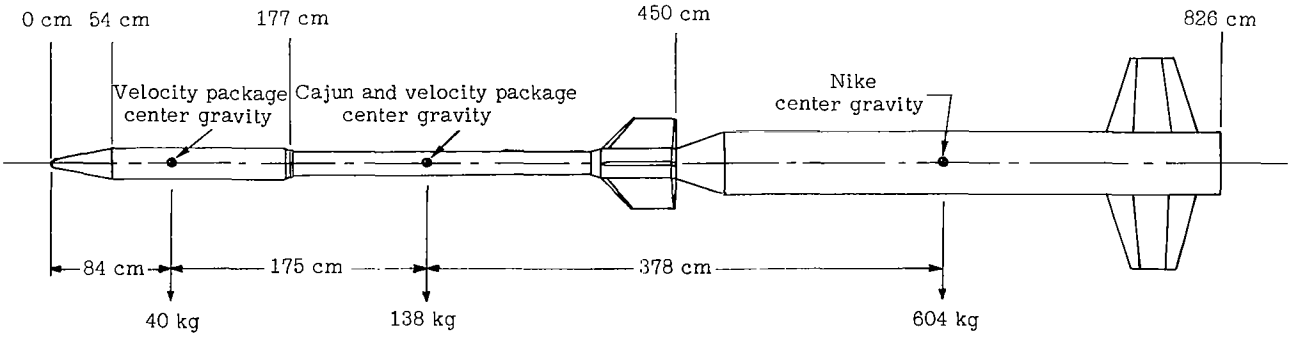

Figure 1.- Sketch of Nike-Cajun vehicle for meteor simulation experiments. Total mass, 782 kg.

Canted fins on the Cajun motor gave it a spin rate of approximately 5 cycles per second. To stabilize the reentry units further, spin motors on the velocity package ignited approximately 2 seconds after separation from the empty Cajun motor and added

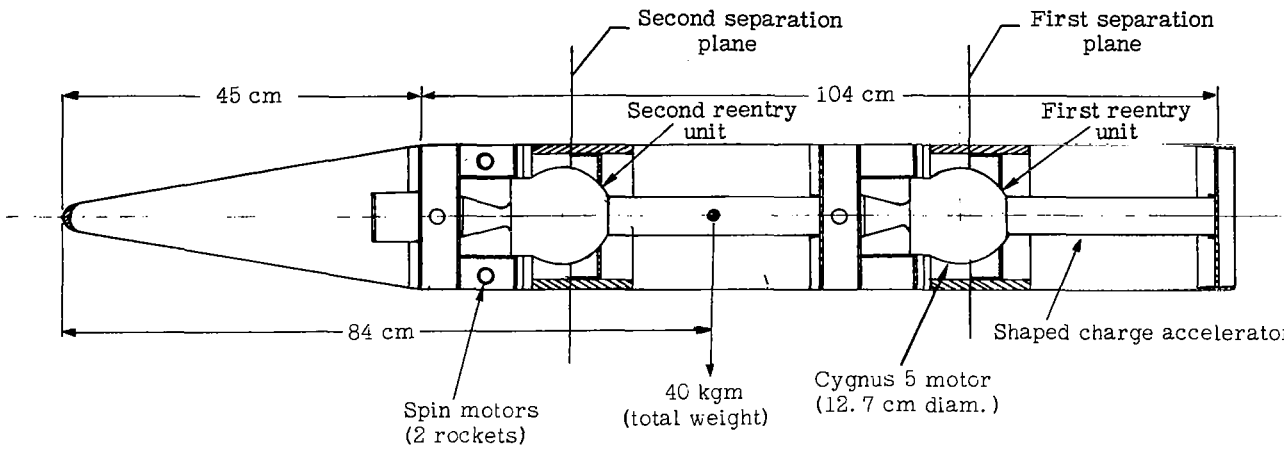

Figure 2.- Sketch of Nike-Cajun velocity package showing reentry stages.

about 20 cycles per second to the spin of the velocity package; thus, it had a total spin rate of 25 cycles per second. The trajectory flown by a typical Nike-Cajun vehicle, and the trajectory of the reentry stages are shown in figure 3.

After burnout, the Nike booster was drag separated from the Cajun motor. Springs separated the velocity package from the Cajun motor after the vehicle left the effective atmosphere at an altitude of about 90 kilometers. This separation was actuated by a programed pyrotechnic device that cut the skin of the velocity package at the first separation plane. (See fig. 2.) After the first reentry unit left the velocity package, a similar timed sequence occurred to cut and spring-separate the velocity package again at the second separation plane; thus, the second reentry unit was permitted to leave the velocity package unobstructed.

Each reentry unit housed inside the velocity package had two stages: a Cygnus 5 rocket motor and a shaped-charge accelerator connected in tandem. The Cygnus 5 motor served two purposes. It separated the shaped-charge accelerator from the velocity package and added from about 1.5 to 1.8 km/sec to the reentry velocity of the meteoroid. The shaped-charge accelerator formed the reentry pellet and added from about 8.0 to 9.5 km/sec to the reentry velocity depending on the characteristics of the accelerator.

Each of the three experiments had one accelerator which formed a nickel meteoroid and another accelerator which formed an iron meteoroid. However, the iron meteor from the third experiment was not observed because of a malfunction in the second reentry unit. This paper reports only the results of the nickel reentries, and no further discussion of the iron reentries from these three experiments is given.

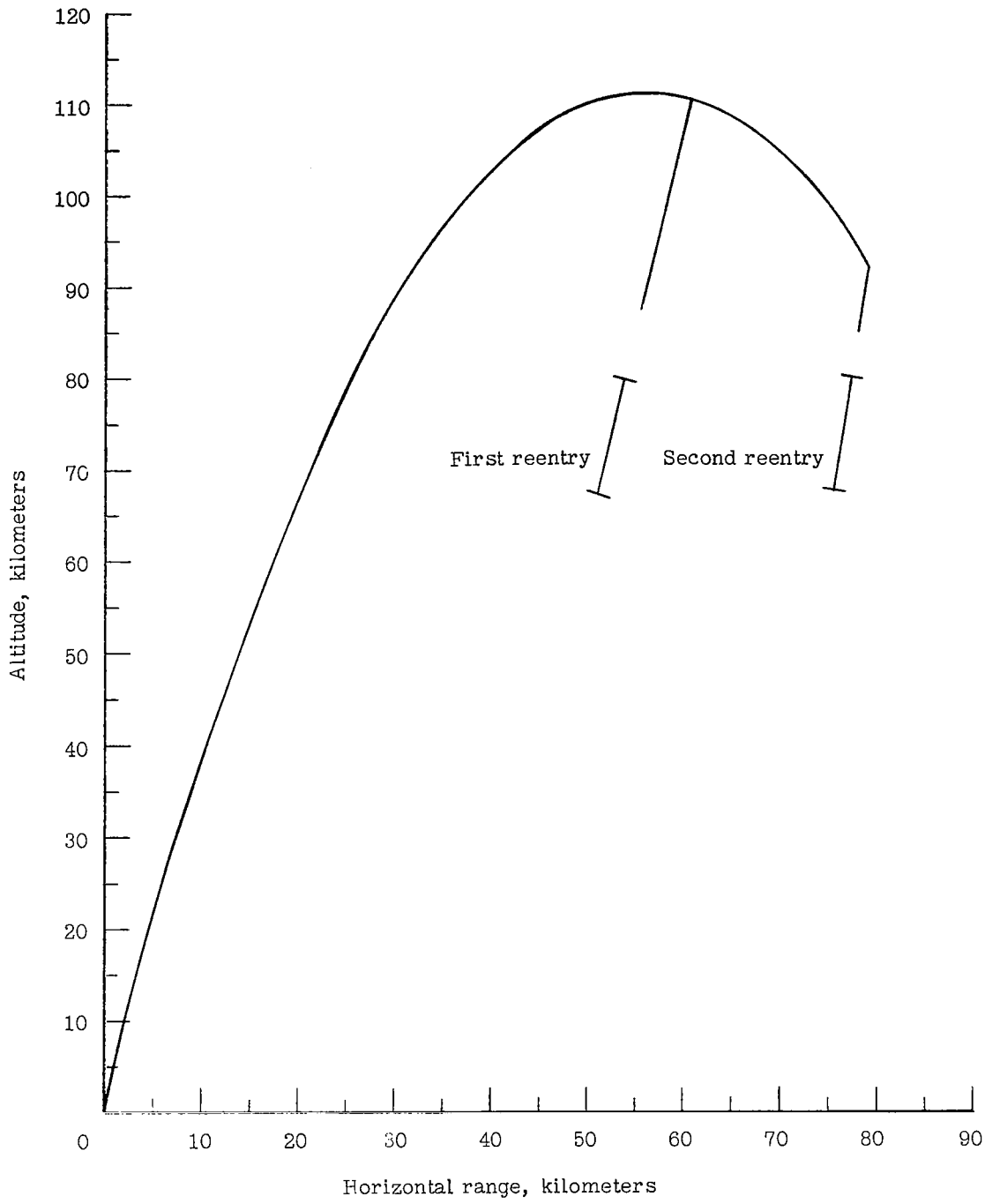

Figure 3.- Nominal trajectory of typical Nike-Cajun for an 80^{0} launch angle.

Shaped-Charge Accelerator

Once the reentry units are boosted to natural meteor altitudes, the requirement of obtaining meteors at high velocities relied on the performance of the shaped-charge accelerator. Figure 4(a) is a drawing of the type accelerator used in the first two nickel reentry experiments. Figure 4(b) is a drawing of the accelerator used in the third nickel reentry experiment. The accelerators have five principal parts: a fiber glass outer body, a booster charge, a nickel liner that forms the pellet, a jet inhibitor, and the main explosive charge. The first two experiments used a 30^{o} conical liner with separate plastic inhibitors. The third experiment had a 40^{o} hyperbolic liner with an inhibitor groove at the base. The shock from the exploding charge collapses the liner and forms a small part of its mass into an irregularly shaped high-velocity pellet. The remainder of the liner mass forms debris and a massive low-velocity slug. The purpose of the inhibitors is to collapse behind the pellet and slow down the low-velocity debris and the slug.

In order to know the mass, velocity, and shape of the nickel pellets, calibration studies to obtain statistical data on the pellets were conducted in a ballistic range. Flash radiographs of the high-speed nickel pellets at low ambient pressures were obtained at two different locations. From these radiographs, velocities, mass, and dimensions were

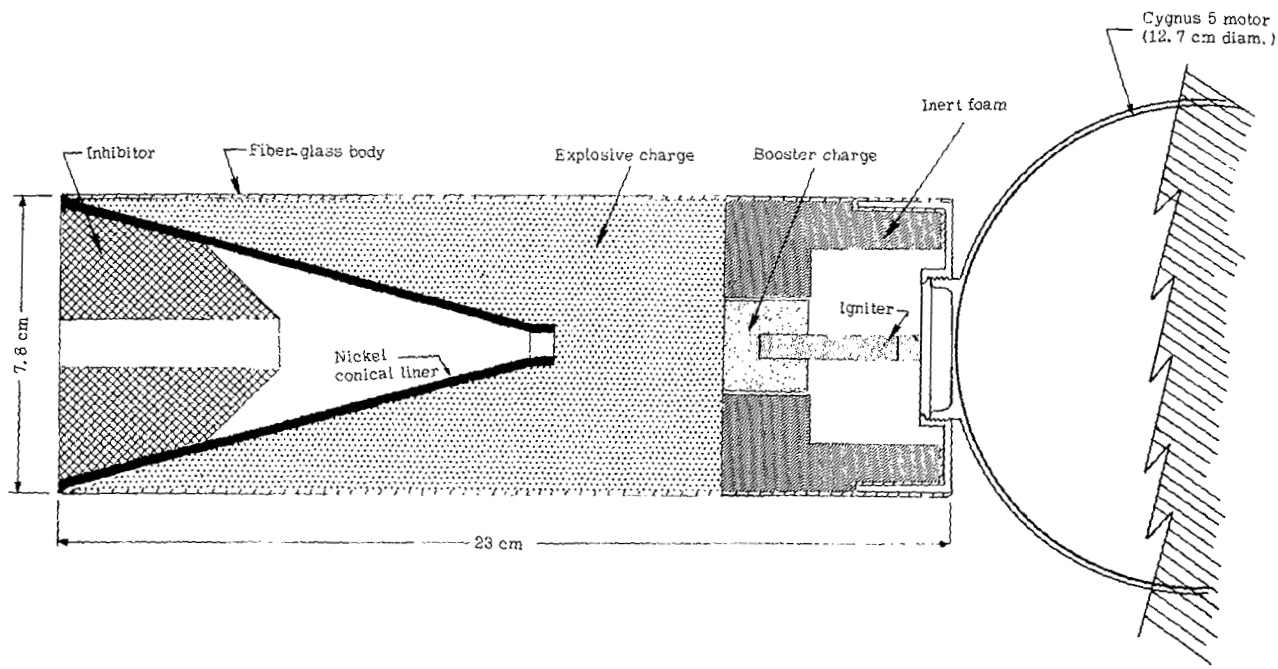

(a) First and second experiment.

Figure 4.- Shaped-charge accelerators used in experiments.

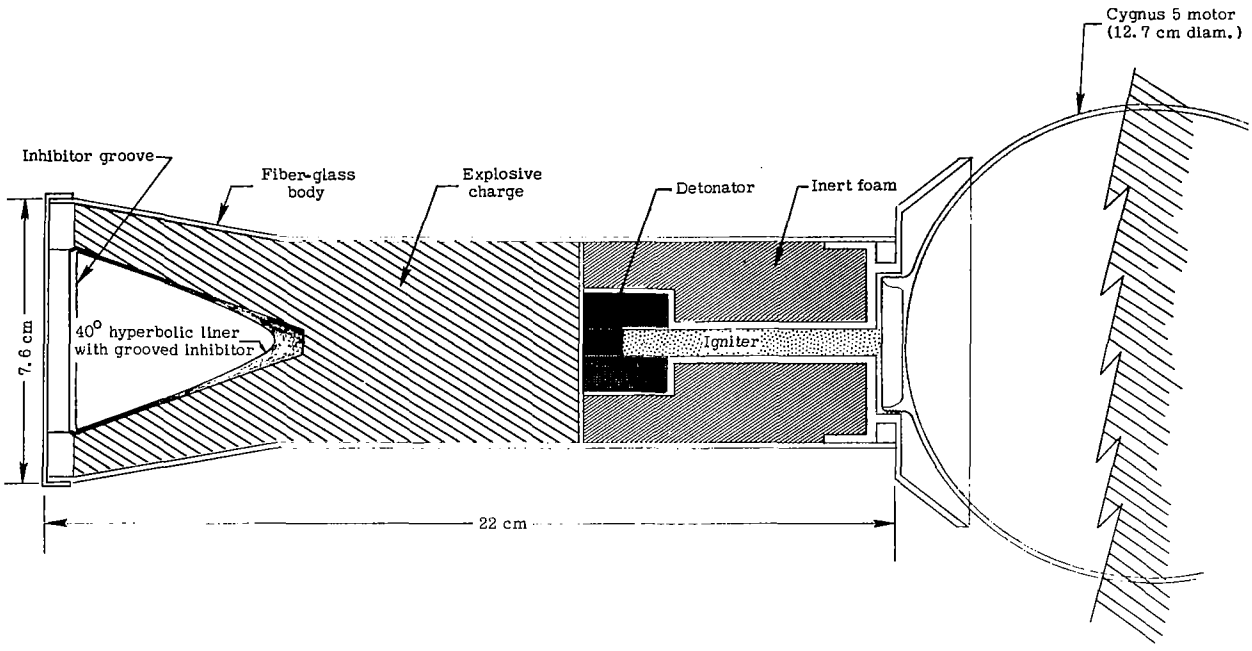

(b) Third experiment.

Figure 4.- Concluded.

determined. The pellet mass, velocity, and dimensions for the first two experiments were based on only seven data points. Similar pellet parameters for the third experiment were based on 18 data points. These parameters for the three experiments are given in table I; flash radiographs of typical nickel pellets are shown in figure 5. Some debris is noticeable around the pellet. References 2 and 3 give a complete discussion of the ground tests and the method used to obtain mass, velocity, and dimensions of the pellets.

TABLE I.- AVERAGE MASS, VELOCITY, AND DIMENSIONS OF TYPE NICKEL PELLETS USED IN THREE REENTRY EXPERIMENTS AS DETERMINED FROM GROUND TESTS

Experiment	Source	Average velocity, km/sec	Average mass, g	Average length, cm	Average diameter, cm
First	Ref. 3 (table IV, station 1, lines 9 to 15; table VI, line 11; table VIII, line 5)	7.94 ± 0.07	1.08 ± 0.12	1.51	0.25
Second	Ref. 3 (table III, station 1, lines 1 to 7; table VI, line 9; table VIII, line 1)	8.60 ± .19	.95 ± .19	1.36	.21
Third	Ref. 2 (table IX, lines 1 to 3; table X, lines 3, 6, and 9)	9.54 ± .02	.88 ± .04	1.00	.38

(a) Typical pellet formed from 30° conical nickel liner, first and second experiment.

(b) Typical pellet formed from 40° hyperbolic nickel liner, third experiment.

L-68-884

Figure 5.- Flash radiographs of nickel pellets formed by ground tests of shaped-charge accelerators.

Photographic Instrumentation

Ground-based ballistic and meteor cameras were used to photograph the luminous reentry trail of the nickel artificial meteors. Camera sites were located at Wallops Island, Virginia; Eastville, Virginia; and Sandbridge, Virginia. The location of the three camera sites with respect to the reentry area is shown in figure 6.

Two photographic systems were employed to measure the luminous power of the nickel artificial meteors; one system designated "panchromatic" consisted of panchromatic film in a K-37 camera with a focal length of 305 mm and an f-number of 2.5. The panchromatic system detects radiation between an estimated 3950 Å and 7000 Å. The short-wavelength cutoff is caused by transmission losses in the K-37 optics. The long-wavelength cutoff is caused by the sensitivity of the panchromatic emulsion.

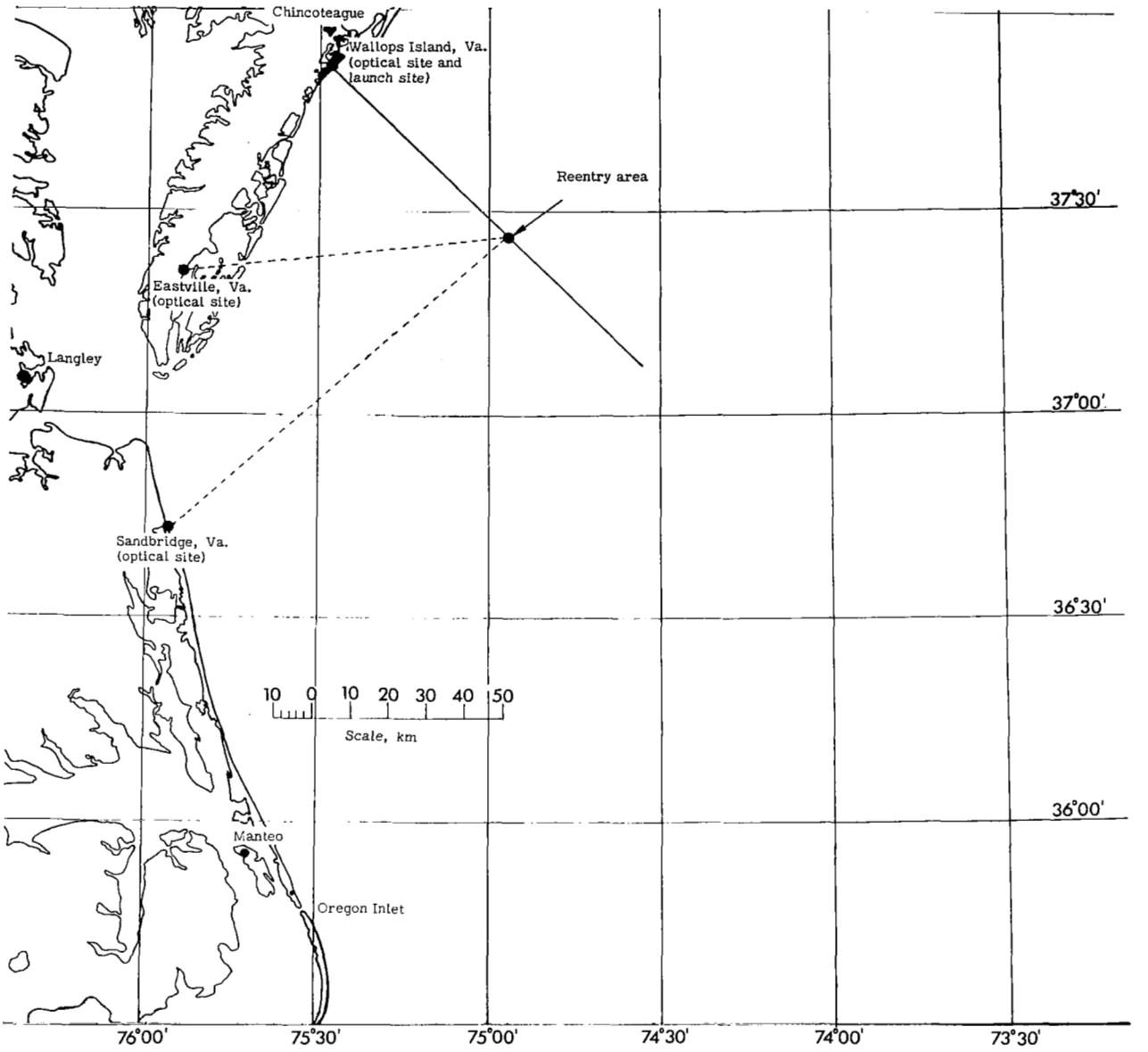

Figure 6.- Camera sites for a typical reentry.

The other system designated "blue" consisted of blue-sensitive film in a Super Schmidt meteor camera, which has a focal length of 203 mm and an effective f-number of 0.85. The blue system detects radiation between approximately 3600 Å and 5200 Å. The short-wavelength cutoff is caused by transmission losses in the camera optics. The Super Schmidt optics transmit more than 50 percent of the radiation at 3800 Å relative to 5000 Å. It is estimated that 5 to 10 percent of the radiation at 3600 Å relative to 5000 Å is passed by the Super Schmidt optics. The Super Schmidt optics pass shorter

wavelength radiation than the K-37 optics; thus, the blue system is sensitive to some ultraviolet radiation not detected by the K-37 camera. The long-wavelength cutoff is caused by the limit of sensitivity of the X-ray emulsion, blue-sensitive film. A more complete discussion of the Super Schmidt camera can be found in reference 4.

PROCEDURE

Basic meteor theory (ref. 1) defines a dimensionless luminous efficiency factor τ_s by assuming that the luminous power I radiated in the visible wavelength band is proportional to the rate of loss of kinetic energy of the ablated atoms. In equation form, this relationship is expressed as

$$I = -\frac{1}{2}\tau_s \frac{dm}{dt} V^2 \tag{1}$$

Recent investigations of natural meteor data indicate that the luminous efficiency τ_s in equation (1) is nearly proportional to the first power of velocity (ref. 5)

$$\tau_s = \tau_o V \tag{2}$$

The meteor magnitude of a point on the meteor trail is defined in terms of the radiant power I at that point by the equation

$$\frac{I}{I_{o,s}} = 10^{-0.4M} \tag{3}$$

where $I_{o,s}$ is the radiant power of a zero magnitude meteor as detected by a system s. For a panchromatic system and a blue system, $I_{o,s}$ has the following values

$$I_{o,p} = 7.96 \times 10^9 \frac{\text{ergs}}{\text{sec}} = 7.96 \times 10^2 \frac{\text{joules}}{\text{sec}}$$

$$I_{o,b} = 5 \times 10^9 \frac{\text{ergs}}{\text{sec}} = 5 \times 10^2 \frac{\text{joules}}{\text{sec}}$$

where the subscript p refers to the panchromatic detector and the subscript b refers to the blue-sensitive detector. (See ref. 6, appendix A.)

It is convenient to express the luminous efficiency in terms of meteor magnitude since this quantity is directly determined from the photographic data. Thus, by dividing

both sides of equation (1) by the radiant power of a zero-magnitude meteor $I_{o,s}$ and substituting equation (2) for τ_s, the result is

$$\frac{I}{I_{o,s}} = 10^{-0.4M} = -\frac{1}{2}\tau'_o \frac{dm}{dt} V^3 \tag{4}$$

where

$$\tau'_o = \frac{\tau_o}{I_{o,s}} = \frac{\tau_s}{I_{o,s}V} \tag{5}$$

Solving equation (4) for τ'_o and integrating the result yield

$$\tau'_o = \frac{2\int 10^{-0.4M} V^{-3} dt}{\int dm} \tag{6}$$

The numerical integration of τ'_o in equation (6) can be represented by

$$\tau'_o = \frac{2}{m}\sum 10^{-0.4M} V^{-3} \Delta t \tag{7}$$

where Δt is the time increment and m is the mass of the meteoroid before any ablation began.

To make the calculation of τ'_o, it is necessary to obtain two relationships from the photographic data: (1) the velocity of the meteor as a function of time and (2) the intensity of the meteor, that is, the meteor magnitude M as a function of time.

The basic procedure used to obtain velocity and position data follows closely that described in reference 7. This procedure is a two-station method in which distances along the reentry trail from some arbitrary zero point are determined from the intersection of two planes, each of which is defined by the station coordinates, and the apparent reentry trail as seen from that station against a star background. For the region of interest, the reentry trail is assumed to be a straight line. The distances along the reentry trail and their associated relative time, as determined from shutter breaks along the trail, are fitted by the method of least squares to an equation of the form:

$$d = a + bt + ce^{kt} \tag{8}$$

where a, b, c, and k are constants to be determined. Once the constants of this equation are established, the velocity and deceleration are determined by differentiation. The position coordinates in space of any point on the trail are also determined by the two intersecting planes.

The absolute magnitude of the meteor M is defined as the apparent stellar magnitude of the meteor at a distance of 100 kilometers and at zenith. The absolute magnitude is obtained by comparing points along the reentry trail with comparison stars of known magnitude around the trail and then making the necessary corrections. These corrections are an atmospheric extinction correction, a range correction to standardize the reentry to 100 kilometers, a trailing velocity correction, and a correction for possible reciprocity failure of the film emulsion. A discussion of absolute magnitude with corrections can be found in reference 7.

RESULTS AND DISCUSSION

Measured Flight Data

In three separate experiments, a Nike-Cajun launch vehicle successfully reentered a nickel artificial meteoroid into the earth's atmosphere. In each experiment, the resulting meteor trail was visible to the naked eye and was photographed by ground-based ballistic and meteor cameras.

The nickel meteor from the first experiment was very faint and was recorded only by the fast (f/0.85) Super Schmidt meteor camera using blue-sensitive X-ray film. No flight velocity measurement was possible because of blending of the chopped trail, possibly because of fragmentation of the meteoroid or the associated debris near the meteoroid. However, for the purpose of calculating luminous efficiency parameters, the reentry velocity was estimated to be 9.8 km/sec from the average measured velocity of ground tests of the shaped-charge accelerator (7.94 $\pm$ 0.07 km/sec) and the average velocity contribution of the Cygnus 5 rocket motor (1.83 km/sec) taken from previous flight experiments. The blue-light curve for this reentry is shown in figure 7.

The nickel meteoroid from the second experiment broke into two large fragments producing very faint meteors of nearly the same brightness, velocity, and duration. The two meteors had an angular separation of approximately 2.5° and a maximum spatial separation of about 1 kilometer during the luminous trail. Velocity measurements were obtained for approximately two-thirds of each of the trails. As in the first experiment, the meteor trails were recorded only by the f/0.85 Super Schmidt meteor camera which used blue-sensitive X-ray film. A Super Schmidt photograph of this nickel reentry is shown in figure 8. The common velocity curve of figure 9 represents only those portions of the trails where velocity measurements could be made. The corresponding light curves

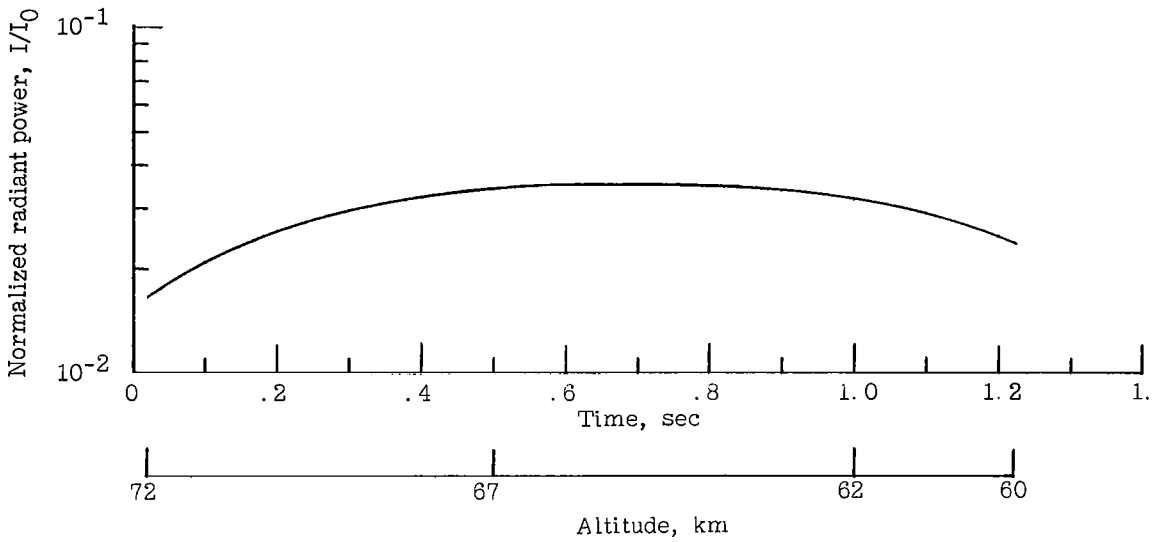

Figure 7.- Blue-light curve of nickel artificial meteor from first nickel reentry experiment. 3600 Å to 5200 Å.

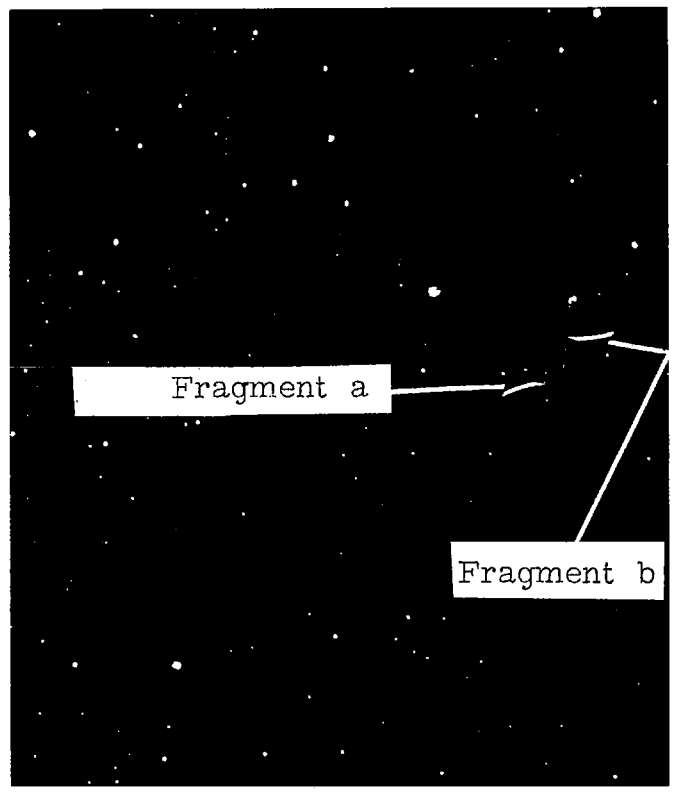

L-68-885

Figure 8.- Super Schmidt photograph of nickel meteor from second experiment. 2X enlargement.

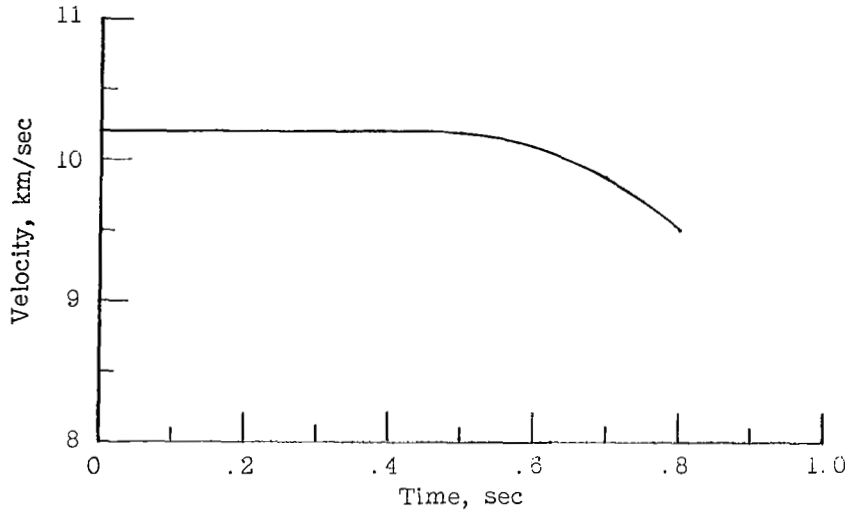

Figure 9.- Velocity time history of nickel meteor from second experiment.

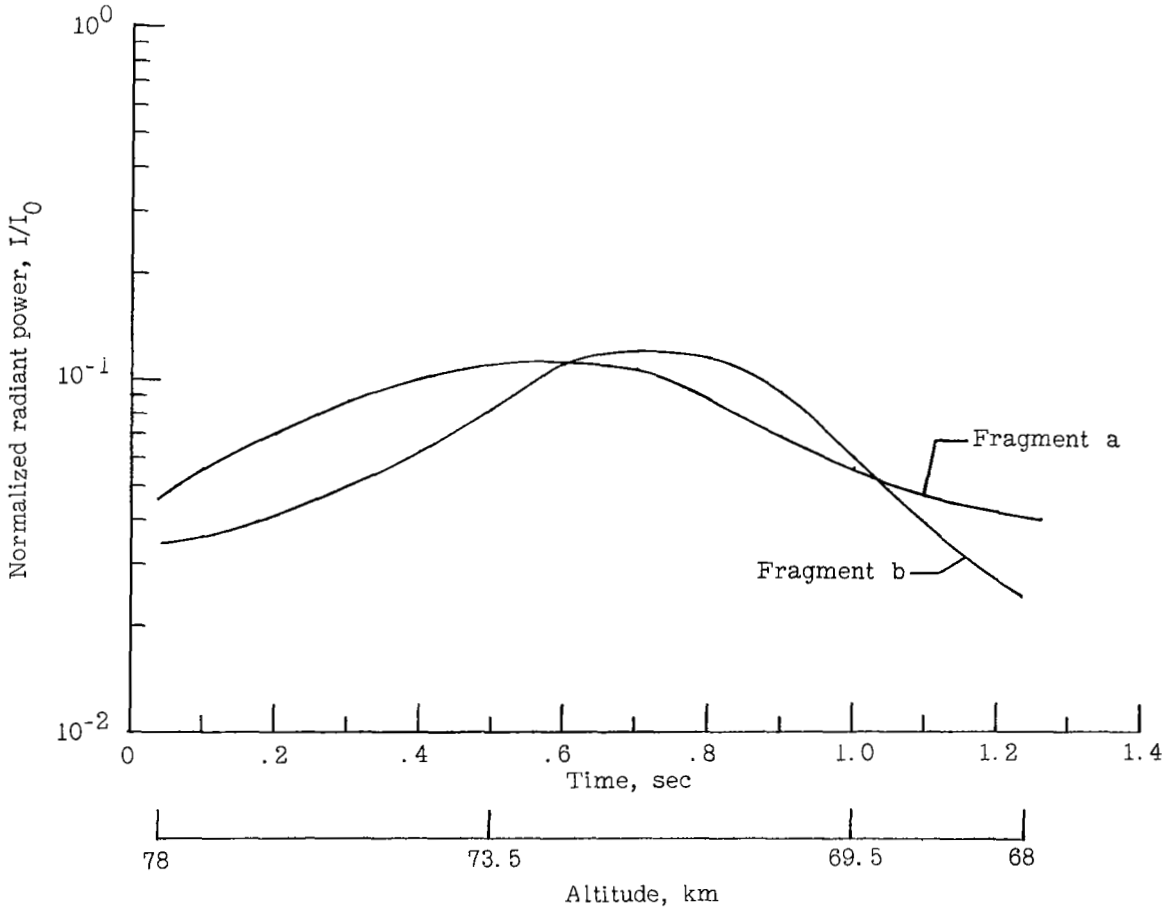

Figure 10.- Blue-light curve of nickel artificial meteor from second nickel reentry experiment. 3600 Å to 5200 Å.

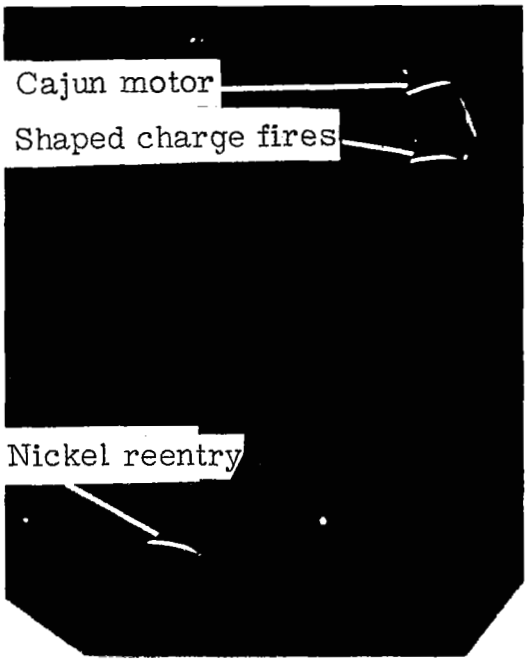

L-68-886
Figure 11.- Super Schmidt photograph of nickel meteor from third experiment. 2X enlargement.

for these meteor fragments are shown in figure 10. Since these two fragments have the same velocity, visible duration, integrated light intensity, and similar shape light curves, their masses were taken as being equal. If it is assumed that no mass loss occurred when the original meteoroid fragmented, luminous efficiencies can be calculated by using the original meteoroid mass.

The nickel meteor from the third experiment was the fastest and brightest of the nickel meteors from the three experiments. It was recorded by the Super Schmidt meteor cameras which used blue-sensitive X-ray film and by several K-37 cameras which were equipped with panchromatic film. A photograph of the reentry from the Super Schmidt camera is shown in figure 11. Velocity measurements were made over most of the visible trail and both blue and panchromatic light curves were obtained. The velocity curve and the light curves are shown in figures 12 and 13, respectively.

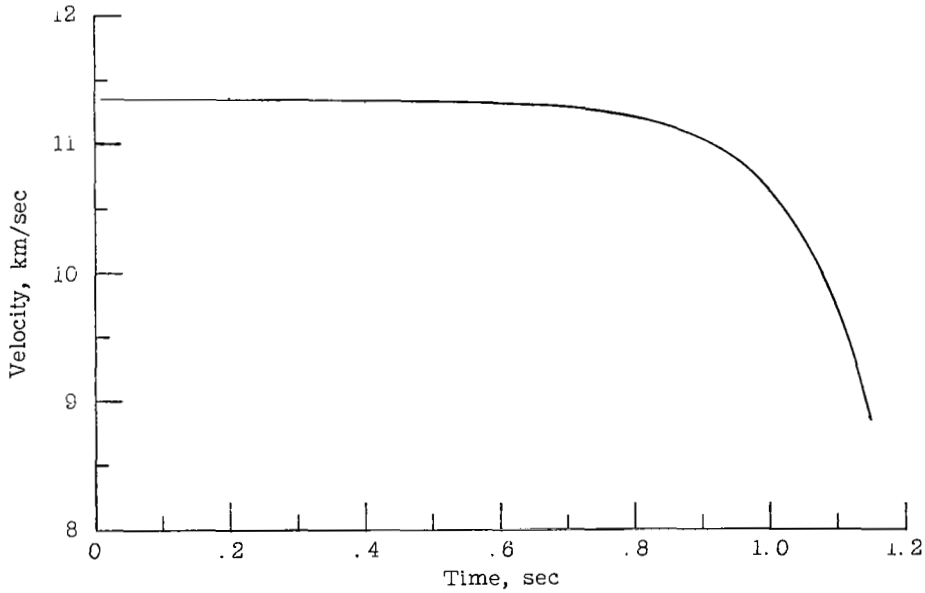

Figure 12.- Velocity time history of nickel meteor from third experiment.

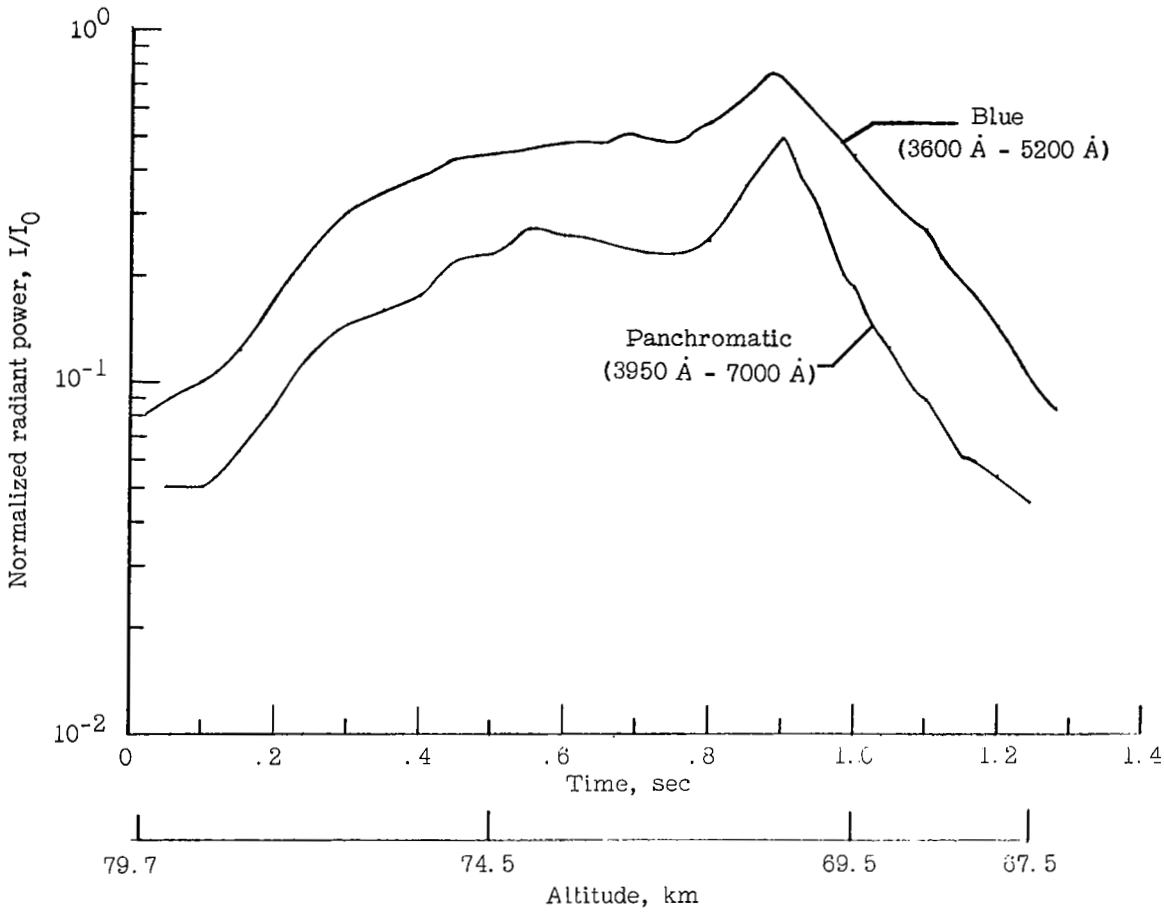

Figure 13.- Light curves of nickel artificial meteor from third nickel reentry experiment.

As shown in figure 13, the two light curves have about the same shape but the blue-light curve is about 0.8 of a magnitude brighter than the panchromatic light curve. Most of this difference in magnitude can be explained on the basis of wavelength radiation. The principal lines of the emission spectra of nickel are most intense in the ultraviolet region from about 3400 Å to 3600 Å. A spectrogram for this nickel meteor indicated that the spectral distribution of the radiation is strongly grouped at 3500 Å of the ultraviolet (ref. 4, appendix B). Thus, the blue-light (3600 Å to 5200 Å) curve obtained from a photograph taken with a Super Schmidt camera that passes a significant amount of light in the ultraviolet is much brighter than the panchromatic light curve. Spectrograms were not available for the meteor reentries of the first two experiments; therefore, the wavelengths at which radiation occurred could not be determined.

By performing numerical integrations of the light curves of the nickel reentries from the three experiments and using equations (1) to (7), the luminous efficiency parameters were obtained and listed in table II.

TABLE II.- LUMINOUS EFFICIENCY PARAMETERS

FOR THREE NICKEL METEORS

Experiment	Velocity, km/sec	$\tau'_{o,s}$, $sec^4/gm\ cm^3$	$\tau_{o,s}$, sec/cm	τ_s
First	*9.8	$\tau'_{o,b}$:0.75×10^{-19}	$\tau_{o,b}$:0.38×10^{-9}	τ_b:$(3.7 \pm 0.9) \times 10^{-4}$
Second	10.4	$\tau'_{o,b}$:3.30	$\tau_{o,b}$:1.65	τ_b:$(1.7 \pm 0.5) \times 10^{-3}$
Third	11.4	$\tau'_{o,b}$:7.95	$\tau_{o,b}$:3.98	τ_b:(4.5 ± 0.9)
Third	11.4	$\tau'_{o,p}$:3.66	$\tau_{o,p}$:2.91	τ_p:(3.3 ± 0.7)

*Estimated velocity.

Based on the quality of the photographic data that were obtained from the three experiments, the luminous efficiency from the third experiment is the most reliable. The luminous efficiency from the first experiment is the least reliable because no velocity measurements were made and there was evidence of fragmentation of the meteoroid.

Luminous Efficiencies of Nickel and Iron

Luminous efficiencies for the three nickel meteors as a function of velocity are shown in figure 14. As a basis for comparison, Öpik's theoretical luminous efficiency curve for a 1-gram compact iron meteor is included (ref. 8). Luminous efficiencies of three iron meteors from previous experiments are shown for comparison purposes. (See refs. 6 and 9.) To be more consistent with the experimental values of luminous efficiency which are either blue or panchromatic values, Öpik's curve has been converted from visual luminous efficiencies τ_v to luminous efficiencies for blue film τ_b. Two theoretical curves are shown: one is for faint meteors, the other for bright meteors. The conversion from τ_v to τ_b is accomplished by applying color corrections of -1 magnitude for faint meteors and -1.8 magnitude for bright meteors (ref. 1) and by using equation (A8a) of reference 6.

The data of figure 14 also indicate that the luminous efficiency of iron and nickel is about the same for a velocity of 11 km/sec. The luminous efficiency for the nickel reentry at an estimated 9.8 km/sec is about a factor of 10 less than the corresponding iron luminous efficiency at the same velocity. This factor indicates a difference in slope for the luminous efficiency curves of nickel and iron at low velocities. However, nothing definite can be said about the slope of the luminous efficiency curve for nickel at higher meteor velocities from these tests, but it is believed that the curve will level off in much the same way as Öpik's theory predicts for iron at higher velocities. Further research

on luminous efficiencies of nickel at higher velocities will be needed to substantiate this result.

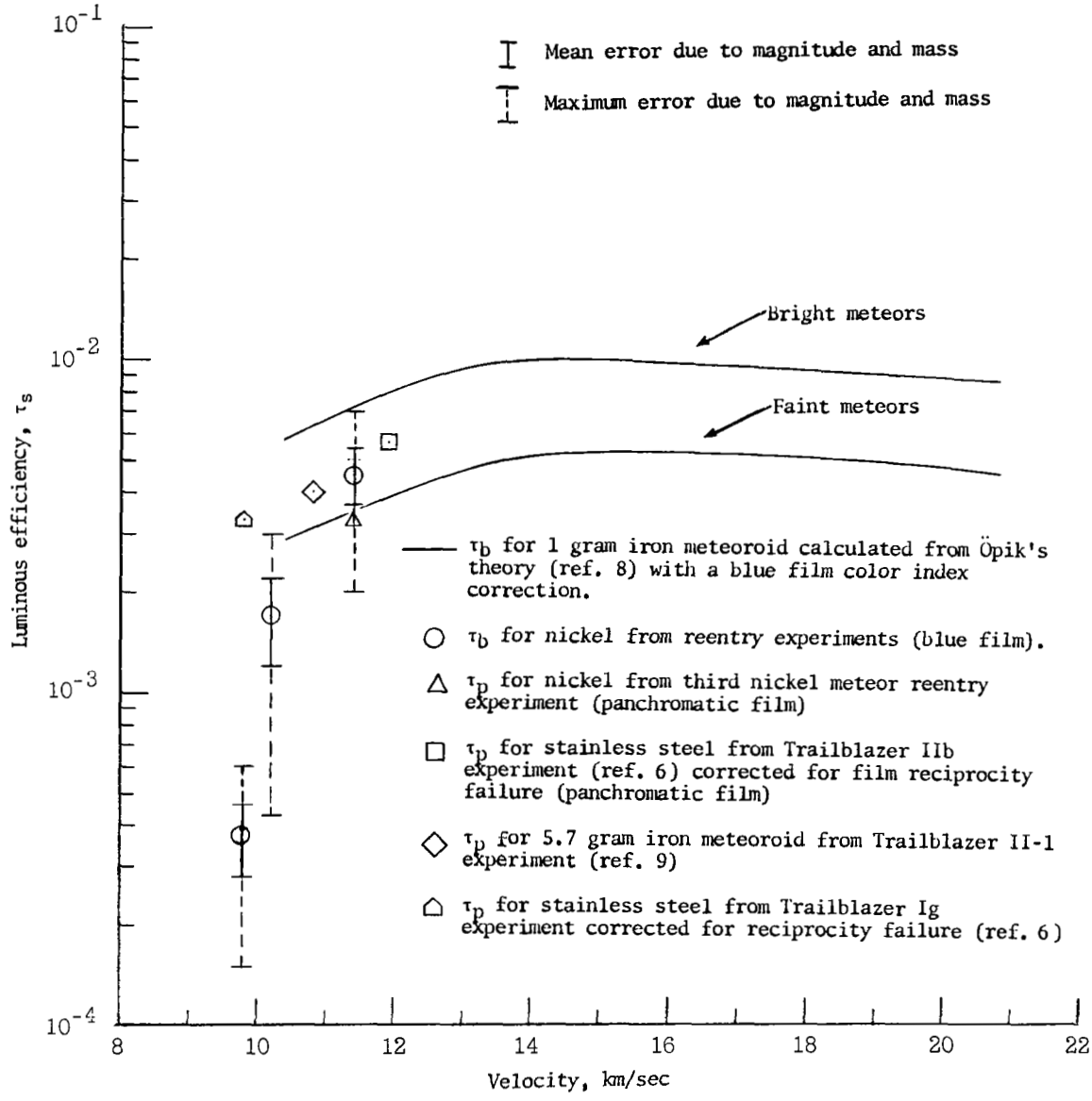

Figure 14.- Luminous efficiency against velocity for iron and nickel meteors.

Errors in the Luminous Efficiency

Uncertainty in meteoroid mass and meteor intensity causes most of the error in luminous efficiency. The uncertainty in mass is due to indirect measurements. The uncertainty in meteor intensity is due to scatter in measured photographic densities of calibration star images on the reentry photograph. The densities of these star images

plotted against their respective stellar magnitudes define a calibration curve from which meteor intensities can be obtained.

The masses of the pellets used to calculate nickel luminous efficiencies for the three nickel experiments are mean masses based on experimental firings in a ground ballistic range equipped with emission X-ray instrumentation at two stations. Orthogonal radiographs of the pellets were taken at the two stations. Data from these radiographs were used to determine pellet masses. References 2 and 3 give complete discussions on determining masses.

In each of the first two experiments the mean mass was based on only seven ground firings. The mean mass of the third experiment was based on 18 ground firings. A listing of the masses of individual pellets for the three experiments is shown in table III.

TABLE III.- INDIVIDUAL MASSES OF NICKEL ARTIFICIAL METEOROIDS USED TO CALCULATE MEAN MASSES FOR THREE EXPERIMENTS

First experiment
Mass, g (station 1)
1.29
.57
1.03
.89
.99
1.22
1.58
Mean: 1.08

Second experiment
Mass, g (station 1)
0.67
.63
.72
.86
1.39
.45
1.94
Mean: 0.95

Third experiment
Mass, g (averaged for stations 1 and 2)
1.05
.82
.70
.82
.82
.72
.75
.70
.68
.66
.96
.85
1.08
1.00
.98
1.22
.98
1.08
Mean: 0.88

Mean masses for the first two experiments were based only on measurements at the first station because the pellets were fired at atmospheric pressure which may have caused ablation by the time the pellet reached the second station. The mean mass for the third experiment was based on measurements at both stations since these pellets were fired at low pressures and no ablation was observed. Pressures varied from 25 to 70 microns and simulated the natural meteor environment. For the first two experiments, the maximum difference between the mean mass and the mass of an individual pellet from the sample is about a factor of 2. For the third experiment the difference is about a factor of 1.4. The mean masses used for the three nickel artificial meteoroids with their standard errors are given in table I. These standard errors indicate the reliability of the mean masses and no mention is made of the mass of a single pellet. Thus, based on the three samples, an individual mass could be different from the mean mass by as much as a factor of 2.

By fitting the calibration curves from each of the three experiments to a straight line by the method of least squares, the uncertainty of the fitted curve was obtained. The maximum uncertainty in density was about ±0.1 over the range of magnitudes. This uncertainty in density corresponded to an error in magnitude of about ±0.2 or a 20-percent change in the luminous efficiency. However, based on the scatter of the density of individual star images about the fitted curve, there could be an error in luminous efficiency of 40 to 50 percent.

The uncertainty in luminous efficiencies for the three experiments due to uncertainties in mean masses and estimated densities is shown in table II and is indicated by the inner error bars in figure 14. The outer error bars (broken lines) indicate the uncertainty in luminous efficiency that could result if the artificial meteoroid masses and density scatter in the calibration curve had maximum deviation from their mean values. For clarity, error bars are not given for the panchromatic luminous efficiency in the third experiment since it has the same percent error as the blue value.

CONCLUDING REMARKS

In three separate experiments, Nike-Cajun rocket vehicles were successful in reentering approximately 1-gram-mass nickel artificial meteoroids back into the earth's atmosphere at velocities ranging from 9.8 to 11.4 km/sec.

Blue-light curves were obtained of the nickel meteors from the three experiments and luminous efficiency parameters were determined. A panchromatic light curve with its corresponding luminous efficiency parameters was obtained for the third nickel experiment. The blue-light curve of the third experiment was about 0.8 of a magnitude or a factor of 2 brighter than the panchromatic light curve with corresponding higher values of

luminous efficiency parameters. This difference was due to predominant ultraviolet radiation of the nickel reentry at 3500 Å, verified by a spectrogram of the reentry. The camera optics used to record the blue records of the reentry was sensitive to some of the ultraviolet radiation, whereas the camera optics used to record the panchromatic records was sensitive to little, if any, ultraviolet radiation. Spectrograms were not available on the first two nickel reentry experiments. Therefore, the wavelengths at which radiation occurred could not be determined.

Comparison of the luminous efficiency of nickel with experimental values of luminous efficiency of iron shows that over the velocity range of these tests, the luminous efficiency of nickel is about the same as that of iron between 11 and 12 km/sec; however, for the two experiments at lower velocities, the luminous efficiency of nickel is as much as a factor of 10 less than the corresponding iron luminous efficiencies.

It is believed that the luminous efficiency of nickel at higher velocities will level off in much the same way Öpik's theory predicts for iron. However, further research on nickel luminous efficiencies at higher velocities will be necessary to substantiate this.

Langley Research Center,
National Aeronautics and Space Administration,
Langley Station, Hampton, Va., April 15, 1968,
709-06-00-01-23.

REFERENCES

1. McKinley, D. W. R.: Meteor Science and Engineering. McGraw-Hill Book Co., Inc., 1961.

2. Woodall, R. L.; and Clark, E. L.: Development and Testing of Advanced Shaped Charge Meteoritic Simulators. Part II – Calibration of Flight Guns. NASA CR-66216, Firestone Tire and Rubber Co., [1966.]

3. Clark, E.: Development and Testing of Shaped Charge Meteoritic Simulators – Calibration Study. Contract NAS 1-4187, Firestone Tire and Rubber Co., Oct. 1965.

4. Harvey, Gale A.: A Description of Four Fast Slitless Spectrographs. NASA TN D-4145, 1967.

5. Verniani, Franco: On the Luminous Efficiency of Meteors. Spec. Rept. No. 145, Smithsonian Inst. Astrophys. Obs., Feb. 17, 1964.

6. Ayers, Wendell G.: Luminous Efficiency of an Artificial Meteor at 11.9 Kilometers Per Second. NASA TN D-2931, 1965.

7. Whipple, Fred L.; and Jacchia, Luigi G.: Reduction Methods For Photographic Meteor Trails. Smithsonian Contrib. Astrophys., vol. 1, no. 2, 1957, pp. 183-206.

8. Öpik, Ernst J.: Physics of Meteor Flight in the Atmosphere. Interscience Publ., Inc., 1958.

9. Robertson, J. B.; and Ayers, Wendell G.: Photometry of an Iron Artificial Meteor Reentering at 11 Kilometers Per Second. NASA TN D-4312, 1968.

NASA-Langley, 1968 —— 30 L-5774